

Field induced spin ice like orders in spin liquid $\text{Tb}_2\text{Ti}_2\text{O}_7$

H. Cao¹, A. Gukasov¹, I. Mirebeau¹, P. Bonville², and G. Dhalenne³.

¹Laboratoire Léon Brillouin, CEA-CNRS, CE-Saclay, 91191 Gif-sur-Yvette, France.

²Service de Physique de l'Etat Condensé, CEA-CNRS, CE-Saclay, 91191 Gif-Sur-Yvette, France. and

³Laboratoire de Physico-Chimie de l'Etat Solide Université Paris-Sud, 91405 Orsay, France.

We have studied the field induced magnetic structures in the spin liquid $\text{Tb}_2\text{Ti}_2\text{O}_7$, in a wide temperature ($0.3 < T < 270$ K) and field ($0 < H < 7$ T) range, by single crystal neutron diffraction with $\mathbf{H} // [110]$ axis. We combined unpolarized neutron data with polarized ones, analyzed within the local susceptibility model. A ferromagnetic-like structure with $\mathbf{k} = 0$ propagation vector is induced, whose local order at low field and low temperature is akin to spin ice. The four Tb ions separate in α and β chains having different values of the magnetic moments, which is quantitatively explained by taking the crystal field anisotropy into account. Above 2 T and below 2 K, an antiferromagnetic-like structure with $\mathbf{k} = (0,0,1)$ is induced besides the $\mathbf{k} = 0$ structure. It shows a reentrant behavior and extends over a finite length scale. It occurs together with a broadening of the nuclear peaks, which suggests a field induced distortion and magnetostriction effect.

PACS numbers: 71.27.+a, 75.25.+z, 61.05.fg

Geometrical frustration now attracts considerable interest, as being a possible tool for tuning several physical properties concomitantly. The pyrochlore lattice of corner sharing tetrahedra offers the best model of this frustration in three dimensions, leading to short range magnetic orders such as spin liquids, spin ices and spin glasses without chemical disorder. $\text{R}_2\text{Ti}_2\text{O}_7$ pyrochlores where $\text{R}=\text{Dy}$ or Ho are model spin ices¹, with a ground state entropy akin to that of real ice². Ho or Dy magnetic moments interact via ferromagnetic first neighbor interactions and are constrained to point along their local $\langle 111 \rangle$ Ising axes. The local spin ice structure, with 6-fold degeneracy, consists of two spins pointing in and two out of each tetrahedron.

The spin ice degeneracy is lifted by a magnetic field H , leading to original magnetic transitions, which depend on the orientation of \mathbf{H} with respect to the local $\langle 111 \rangle$ trigonal axes³. With $\mathbf{H} // [111]$, magnetization plateau and liquid-gas transition occur^{4,5,6}, providing the first evidence of magnetic monopoles⁷. Applying $\mathbf{H} // [100]$ yields the first magnetic example⁸ of the Kasteleyn transition known in polymers. With $\mathbf{H} // [110]$, the lattice divides into α and β chains^{9,10,11}, with different angles between \mathbf{H} and the local Ising axes.

In $\text{Tb}_2\text{Ti}_2\text{O}_7$, the crystal field (CF) anisotropy is weaker than in canonical spin ices, and ferromagnetic (F) and antiferromagnetic (AF) first neighbor interactions nearly compensate. This widely studied spin liquid^{12,13}, where short range correlated moments fluctuate down to 50 mK, was also called a "quantum spin ice"¹⁴. Its magnetic ground state (GS) is very sensitive to perturbations. Lattice expansion induced by substituting Sn for Ti yields a long range "ordered spin ice" in $\text{Tb}_2\text{Sn}_2\text{O}_7$ ¹⁵. An AF long range order (LRO) is induced under applied stress and/or magnetic field^{16,17,18}.

Up to now, the complex field induced magnetic structures were not studied precisely in $\text{Tb}_2\text{Ti}_2\text{O}_7$. We have combined high accuracy neutron diffraction experiments with both polarized and unpolarized neutrons, in a wide temperature ($0.3 < T < 270$ K) and field ($0 < H < 7$ T) range, to investigate them in detail. The polarized neutron technique, newly used for such compounds, allows very small moments to be measured with great accuracy, which is crucial for low fields and

high temperatures. It yields microscopic information on the magnitude and orientation of the field induced ordered moments. Our data analysis is based on the local susceptibility approach¹⁹. We show that it is valid in fields up to 1 T, and temperatures $5 < T < 270$ K. It takes advantages of the high symmetry of the pyrochlore lattice which allows us to refine these complex magnetic structures with only two parameters, for any orientation of the magnetic field.

For all temperatures and fields $\mathbf{H} // [110]$, we observe an F-like structure with propagation vector $\mathbf{k} = 0$, characterized by magnetic Bragg peaks of the face centered cubic lattice. We show that it involves α and β -chains as in model spin ices. But in $\text{Tb}_2\text{Ti}_2\text{O}_7$, these chains have very different moment values. This original effect is described quantitatively using the CF parameters derived in Ref.20. It provides a nice example of different moments induced by the field on the same crystallographic sites of a homogeneous and highly symmetric lattice.

Below 2 K and for fields above 2 T, we also observe a second family of Bragg peaks, belonging to the simple cubic lattice¹⁸. They are indexed in the cubic unit cell of $Fd\bar{3}m$ space group with a propagation vector $\mathbf{k} = (0,0,1)$. We studied this AF-like structure down to 0.3 K in fields up to 7 T, using unpolarized neutrons. We discuss its observation together with the F-like structure and propose an explanation for its origin. The whole analysis provides a microscopic description of the field induced magnetic structures in $\text{Tb}_2\text{Ti}_2\text{O}_7$.

The neutron diffraction studies were performed on the diffractometer Super-6T2 at the Orphée reactor of the Laboratoire Léon Brillouin²¹. The field was applied close to a $\langle 110 \rangle$ axis, with a misorientation of 5° . We used unpolarized neutrons of wavelength $\lambda_n = 0.90$ Å, collecting 200 reflections for each (H, T) set, for 10 temperatures between 0.3 K and 50 K and 7 fields between 0 and 7 T. We also used polarized neutrons of incident wavelength $\lambda_n = 0.84$ Å and polarization $P_0 = 0.91$. We collected flipping ratios at 200 to 400 Bragg peaks for each (H, T) set, for 8 temperatures between 5 and 270 K, in a field of 1 T. The programs FULLPROF²² and CHILSQ²³ were used to refine the magnetic intensities and flipping ratios, respectively.

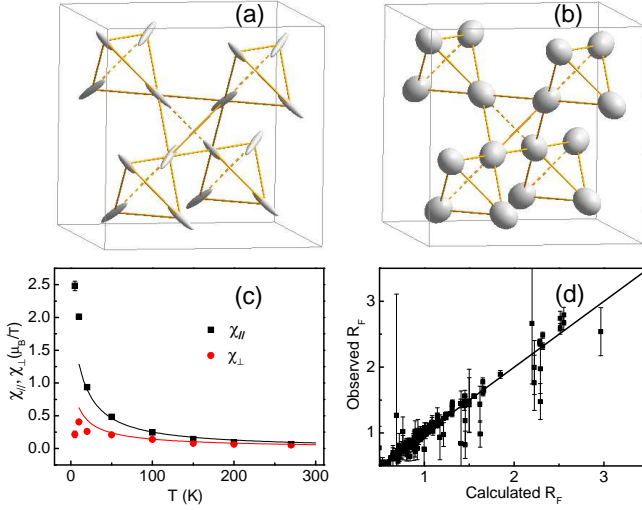


FIG. 1: (Color online) $\text{Tb}_2\text{Ti}_2\text{O}_7$: Local anisotropic susceptibility ellipsoids $\chi_{ij}T$, measured at 10 K (a) and 270 K (b). Ellipsoids were scaled by temperature to compensate the Curie behavior of the susceptibility. (c) susceptibility components χ_{\parallel} and χ_{\perp} versus T . The lines are calculations using the CF parameters of $\text{Tb}_2\text{Ti}_2\text{O}_7$ (see text); d: Measured versus calculated flipping ratio at 10 K; the refinement carried out with $\mathbf{H}=1 \text{ T} // [110]$ on 423 flipping ratios gave $\chi_{11}=0.939(15) \mu_B/\text{T}$ and $\chi_{12}=0.535(11) \mu_B/\text{T}$ with the goodness of fit $\chi^2=2.92$.

A single crystal of $\text{Tb}_2\text{Ti}_2\text{O}_7$ was grown by the floating-zone technique. Its crystal structure was refined at 50 K within the $Fd\bar{3}m$ space group (434 reflections measured in zero-field), in agreement with powder data²⁵.

In the pyrochlore lattice, the 16 Tb atoms of the cubic unit cell occupy a single site ($16d$) with local symmetry $\bar{3}m$. They can be subdivided into 4 different groups according to the directions of their local $\langle 111 \rangle$ anisotropy axes. For $\mathbf{H} // [110]$ the $Fdd2$ group must be used in the magnetic moment refinement¹⁹. It is the highest symmetry subgroup of the $Fd\bar{3}m$ space group which leaves the magnetization invariant. In this subgroup the $16d$ sites split into two different subsets corresponding to the α -chains (where \mathbf{H} makes an angle of 35.3° with the local $\langle 111 \rangle$ easy axis) and to the β -chains (where it is perpendicular), respectively.

In the local susceptibility approach¹⁹, the atomic site susceptibility tensor accounts for the linear paramagnetic response of the moments to an applied field of arbitrary direction. The induced magnetic moment \mathbf{M}^d at the $16d$ site of the unit cell writes: $\mathbf{M}^d = \bar{\chi}^d \mathbf{H}$, where $\bar{\chi}^d$ is a tensor of rank 3×3 , whose components χ_{ij} depend on the symmetry of the atomic site. The magnetic moments are in general not parallel to the field, and the magnetic structure is not necessarily collinear, as reflected by the non diagonal terms in the susceptibility tensor. In the cubic axes, the symmetry constraints on the susceptibility tensor for a magnetic atom at the $16d$ site in the $Fd\bar{3}m$ group imply: $\chi_{11} = \chi_{22} = \chi_{33}$; $\chi_{12} = \chi_{13} = \chi_{23}$. So only two independent parameters need to be determined regardless of the field direction. The susceptibility components χ_{\parallel} and χ_{\perp} , respectively parallel or perpendicular to the local $\langle 111 \rangle$

easy axis, measure the anisotropy on a given Tb ion. They are given by the relations: $\chi_{\parallel} = \chi_{11} + 2\chi_{12}$ and $\chi_{\perp} = \chi_{11} - \chi_{12}$.

We determined the susceptibility components by performing a least square fit of the site susceptibility model to the flipping ratios measured for $\mathbf{H}=1 \text{ T} // [110]$. The refinement at 10 K (Fig. 1d) shows the excellent quality of the fit. The magnetic ellipsoids determined from the site susceptibility parameters are shown in Fig. 1a and 1b at 10 K and 270 K. For a given ellipsoid, the radius vector gives the magnitude and direction of the magnetic moment induced by a field rotating in space. The elongation of the ellipsoid increases with decreasing T , reflecting the increasing CF anisotropy, as the magnetic moments evolve from Heisenberg to Ising behavior, being more and more constrained to align along their local $\langle 111 \rangle$ axes. At 10 K the two components χ_{\parallel} and χ_{\perp} (Fig. 1c) along the easy and hard local axes differ by a factor 5. They still differ up to 200 K, but become practically equal at 270 K. The lines in Fig. 1c were calculated using the CF interaction in $\text{Tb}_2\text{Ti}_2\text{O}_7$ ²⁰, with a magnetic field of 1 T applied either parallel or perpendicular to the local $\langle 111 \rangle$ axis. Good agreement with the data requires the AF exchange to be taken into account: using a self-consistent calculation, valid down to $\sim 10 \text{ K}$, we obtain a molecular field constant $\lambda = -0.35 \text{ T}/\mu_B$, close to the value derived in Ref.20.

Once the site susceptibility parameters are known, one can easily calculate the magnitude and the direction of the moments induced on each Tb site by a field applied in an arbitrary direction. This approach is valid for fields of 1 T and temperatures $5 < T < 270 \text{ K}$, a range where the susceptibility parameters obey a Curie-Weiss law (Fig. 1c). Below $\sim 5 \text{ K}$, the local susceptibility approach is no longer valid and we used unpolarized neutron diffraction to determine the magnetic structure. We refined the unpolarized neutron data assuming 4 different moments (in magnitude and orientation) on the 4 independent Tb sites of the cubic unit cell. The values plotted in Fig. 2 for $\mathbf{H} = 1 \text{ T} // [110]$ combine the analysis from polarized neutrons, for $5 < T < 270 \text{ K}$, and unpolarized neutrons for $0.3 < T < 10 \text{ K}$. The two sets of data show a perfect overlap.

For $\mathbf{H}=1 \text{ T} // [110]$, the $\mathbf{k} = 0$ structure (Fig. 2a) at 0.3 K clearly shows a local spin ice order, with two moments pointing in and two out of a given tetrahedron. All moments keep close to their $\langle 111 \rangle$ easy axis. The four tetrahedra of the unit cell are the same, as in $\text{Tb}_2\text{Sn}_2\text{O}_7$ ordered spin ice¹⁵. But in striking contrast with standard spin ice structures, here the Tb moments have very different magnitudes (Fig. 2b). The α -moments reach $5.7(3) \mu_B$ at 0.3 K, close to the $5.7(2) \mu_B$ value deduced from the crystal field study²⁰, whereas the β -moments only reach $1-2 \mu_B$. The angular dependencies (not shown here), show that α -moments keep close to their local $\langle 111 \rangle$ easy axis up to about 3 K, then reorient smoothly along \mathbf{H} with increasing T . The β -moments remain perpendicular to \mathbf{H} up to about 3 K, then reorient abruptly along \mathbf{H} .

The presence of two types of β moments (β_1 and β_2) with different values can be attributed to the misorientation of \mathbf{H} with respect to the $[110]$ axis (5°). At 1 T and 0.3 K, our refinements yield β -moment values of $0.8(2)$ and $1.3(2) \mu_B$. In contrast, the two types of α -moments keep almost the same values.

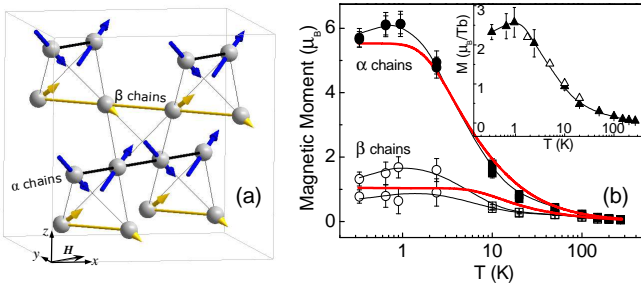


FIG. 2: (Color online) $\text{Tb}_2\text{Ti}_2\text{O}_7$: (a) field induced $\mathbf{k} = 0$ F-like structure at 0.3 K ($\mathbf{H} = 1\text{T} // [110]$). Balls and arrows represent Tb ions and moments, respectively. (b) temperature dependence of the Tb moments from unpolarized (\bullet for α -chains and \circ for β -chains) and polarized (\blacksquare for α -chains and \square for β -chains) neutron data. The two β moments arise from the 5° field misorientation. The thick red lines are a crystal field calculation with a field $H=1$ T applied at 35.3° (resp. 90°) from the local $[111]$ axis for α (resp. β) sites. Inset: magnetization M versus temperature: (\blacktriangle) from the neutron data, (\triangle) from bulk measurements of Ref.20. Thin solid lines are guides to the eye.

The induced α and β -moments vary with temperature as predicted by the crystal field level scheme of $\text{Tb}_2\text{Ti}_2\text{O}_7$ ²⁰, in the whole T range 0.3-270 K (Fig. 2b). In the calculation, the field of 1 T was taken exactly along $[110]$ axis, so one needs to average the measured β -moments to compare with the calculated ones. The agreement is quite good. It shows that the non-zero β -moments found in the $\mathbf{k} = 0$ structure, not seen in model spin ices¹¹, result from the weaker Tb anisotropy and not from the field misorientation. A more sophisticated model should involve both applied and internal fields, and their precise orientations with respect to the crystal axes. We note that different β_1 and β_2 moments are predicted by a CF calculation taking the field misorientation into account. At low temperature, the strongly Ising character should render the β -moments much more sensitive to the field orientation than the α -moments (Fig. 15 of ref. 20), as observed. Knowing the α and β -moments, one can also calculate the average magnetization M in one tetrahedron, (Fig. 2b inset), which perfectly agrees with the bulk magnetization data²⁰.

When \mathbf{H} increases, the moment values in the $\mathbf{k} = 0$ structure increase (Fig. 4a), and their angles with \mathbf{H} decrease, showing that they reorient along the field. The F α -moments quickly saturate, whereas the F β -moments increase more slowly with \mathbf{H} , reaching $3.2(3)\mu_B$ and $6.0(3)\mu_B$ for β_1 and β_2 , respectively, at 7 T and 0.3 K.

For $\mathbf{H} > 2$ T and below 2 K, new magnetic peaks appear, much weaker than the previous ones, indexed in the space group $Fd\bar{3}m$ with $\mathbf{k}=(0,0,1)$. We refined this new family of peaks as a second magnetic structure, also involving the whole sample, and analyzed independently. The $\mathbf{k}=(0,0,1)$ value means that in the cubic cell, two tetrahedra have the same moment orientations and the other two are reversed, so that this AF-like structure has no net magnetization. In the $\mathbf{k}=(0,0,1)$ structure, only the AF β -moments are significant, the AF α -moments are negligible (Fig. 3a and 3b). At 0.3 K, up to $H=7$ T, the AF β -moments remain oriented at $10(5)^\circ$ from

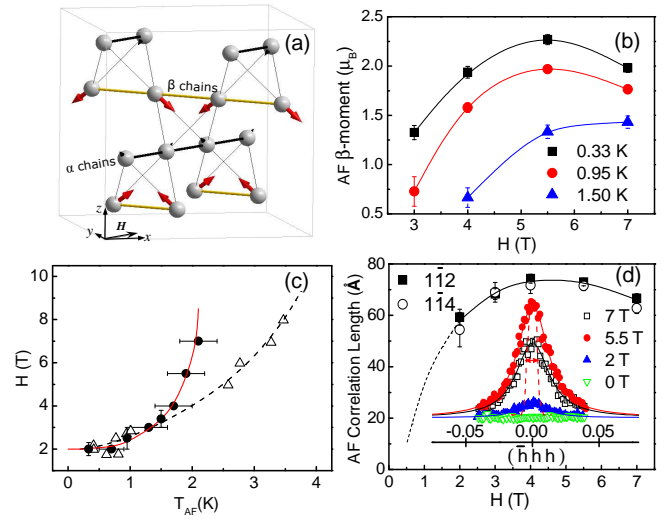


FIG. 3: (Color online) $\text{Tb}_2\text{Ti}_2\text{O}_7$: (a) field induced $\mathbf{k} = (0,0,1)$ AF-like structure at 0.3 K, ($\mathbf{H} = 7\text{T} // [110]$). (b) field dependence of the β moments in the AF-like structure; the α moments (not plotted) are below $0.2\mu_B$. (c) (H, T_{AF}) transition line (\bullet) our measurements, (\triangle) from Ref.18. (d) AF correlation length versus H ; in inset, the $(1\bar{1}2)$ peak for several fields. Solid lines are fits with a Lorentzian peak shape, and dashed line is the resolution peak shape.

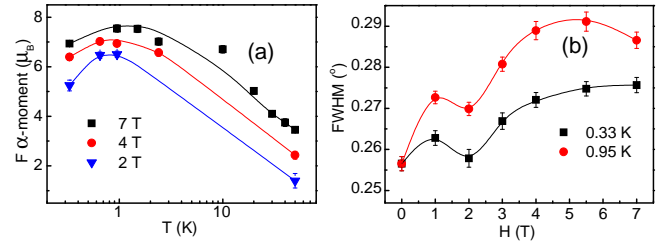


FIG. 4: (Color online) $\text{Tb}_2\text{Ti}_2\text{O}_7$: (a) temperature dependence of the α -moments in the F-like structure in high fields ($H > 2$ T). The F α -moments increase with H and decrease with T below ~ 2 K when the AF-like structure settles in. (b) Field dependence of the full width half maximum (FWHM) of the (440) peak with negligible magnetic contribution. The value at $H=0$ is the resolution limit.

their local $\langle 111 \rangle$ axis, and $90(5)^\circ$ from the field.

The $\mathbf{k}=(0,0,1)$ structure is stabilized in a certain (H, T) range, determined by plotting the peak integrated intensities versus T or H . This yields the transition line $T_{AF}(H)$ plotted in Fig. 3c. It agrees with a previous determination¹⁸ for $0.3 < T < 1.5$ K, but deviates above. The $\mathbf{k}=(0,0,1)$ structure has a finite correlation length ξ_{AF} , as shown by the Lorentzian linewidth of the magnetic peaks (Fig. 3d). ξ_{AF} starts increasing with H , saturates at about 70 \AA around 4 T, then decreases. Its variation reflects that of the AF β -moments (Fig. 3a), suggesting a reentrant behavior. This AF-like structure should disappear at very high fields, where all Tb moments are aligned.

We now summarize the field induced GS in $\text{Tb}_2\text{Ti}_2\text{O}_7$. Below 2 T, the GS consists of a LRO $\mathbf{k}=0$ structure, with field induced moments both on α and β -chains. The moments val-

ues are well explained by CF calculations. The Tb anisotropy, much weaker than in model spin ices, yields non-zero moments on the β -chains. Above 2 T, the GS is a superposition of two modes with $\mathbf{k}=0$ and $(0,0,1)$, the latter ordering with a finite length scale. The $\mathbf{k}=(0,0,1)$ structure occurs together with a decrease of the F α -moments in the $\mathbf{k}=0$ structure (Fig. 4a) and the onset of well defined spin waves¹⁸. It is also connected with a field broadening of the *nuclear* Bragg peaks (Fig. 4b), suggesting a lattice distortion. All these features reflect a symmetry breaking with respect to the quantum spin ice state¹⁴ stable at $H=0$.

The $\mathbf{k}=(0,0,1)$ structure induced by $H// [110]$ strongly resembles that induced by a stress along the same direction¹⁷. This strongly suggests that this structure is induced by magnetostriction effects. For $H=0$, a small distortion was observed in $\text{Tb}_2\text{Ti}_2\text{O}_7$ below 20 K, likely precursor of a Jahn-Teller transition²⁴. In applied field, taking the bulk modulus²⁷ ($B_0=156$ GPa) and volume magnetostriction²⁶ of $\text{Tb}_2\text{Ti}_2\text{O}_7$ at 4 K, we estimate that a field of 7 T is equivalent to a pressure of 0.03 GPa, well below the stress of 0.2 GPa that induces the AF order¹⁷. However this estimation based on the isotropic volume is only a lower estimate for the stress. In $\text{Tb}_2\text{Ti}_2\text{O}_7$, magnetostriction coefficients $//$ and $\perp \mathbf{H}$ have very high values (up to $5 \cdot 10^{-4}$), of opposite signs which nearly

compensate in the isotropic volume magnetostriction. The strong anisotropic magnetostriction arises from the specific Tb crystal field. The sample length $// \mathbf{H}$ expands whereas that $\perp \mathbf{H}$ contracts²⁶. At a microscopic scale, one could speculate that bonds in α -chains expand, weakening the near neighbor exchange interaction J_{nn} along these chains, whereas bonds in β -chains contract, reinforcing J_{nn} . This could explain the AF field induced periodicity along the β -chains.

In conclusion, we determined the field induced magnetic structures in $\text{Tb}_2\text{Ti}_2\text{O}_7$ by combining polarized and unpolarized neutron diffraction, in a wide temperature and field range ($\mathbf{H}// [110]$). The low field GS consists in a $\mathbf{k}=0$ (F-like) structure, with the local structure of a spin ice, but with Tb moments of very different magnitudes. With increasing field, the Tb moments reorient from the spin ice easy axes to the field axis. Above 2 T, a $\mathbf{k}=(0,0,1)$ (AF-like) structure is also stabilized. It exists in a limited (T, H) range, has a finite length scale and shows reentrant behavior. It is attributed to magnetostriction. As temperature increases, the susceptibility ellipsoids show a progressive change from Ising to Heisenberg behavior. This change is demonstrated using the local susceptibility approach, and well explained by the crystal field anisotropy of the Tb ion.

-
- ¹ S. T. Bramwell and M. J. P. Gingras, *Science* **294**, 1495 (2001).
² A. P. Ramirez *et al.* *Nature* **399**, 333 (1999).
³ M. J. Harris *et al.* *Phys. Rev. Lett.* **81**, 4496 (1998).
⁴ K. Matsuhira, Y. Hinatsu, T. Sakakibara *J. Phys.:Condens. Matter* **13**, L737 (2001).
⁵ T. Sakakibara *et al.* *Phys. Rev. Lett.* **90**, 207205 (2003).
⁶ Y. Tabata *et al.* *Phys. Rev. Lett.* **97**, 257205, (2006).
⁷ C. Castelnovo, R. Moessner, S. L. Sondhi, *Nature* **451**, 42 (2008).
⁸ L. D. C. Jaubert *et al.* *Phys. Rev. Lett.* **100**, 067207 (2008).
⁹ Z. Hiroi, K. Matsuhira and M. Ogata, *J. Phys. Soc. Jpn.* **72**, 3045 (2003).
¹⁰ J. P. C. Ruff, R. G. Melko, M. J. P. Gingras, *Phys. Rev. Lett.* **95**, 097202 (2005).
¹¹ T. Fennell *et al.* *Phys. Rev. B* **72**, 224411 (2005).
¹² J. S. Gardner *et al.*, *Phys. Rev. Lett.* **82**, 1012 (1999).
¹³ M. Enjalran and M. J. P. Gingras *Phys. Rev. B* **70**, 174426 (2004).
¹⁴ H. R. Molavian, M. J. P. Gingras, and B. Canals, *Phys. Rev. Lett.* **98**, 157204 (2007).
¹⁵ I. Mirebeau *et al.* *Phys. Rev. Lett.* **94**, 246402 (2005).
¹⁶ I. Mirebeau *et al.* *Nature* **420**, 54 (2002).
¹⁷ I. Mirebeau *et al.* *Phys. Rev. Lett.* **93**, 187204 (2004).
¹⁸ K. C. Rule *et al.* *Phys. Rev. Lett.* **96**, 177201 (2006).
¹⁹ A. Gukasov and P. J. Brown. *J. Phys. Condens. Matter* **14**, 8831, (2002).
²⁰ I. Mirebeau, P. Bonville, and M. Hennion, *Phys. Rev. B* **76**, 184436 (2007).
²¹ A. Gukasov *et al.* *Physica B* **397**, 131134 (2007).
²² J. Rodríguez-Carvajal, *Physica B* **192**, 55 (1993).
²³ P. J. Brown and J. C. Matthewman, CCSL-RAL-93-009 (1993), and <http://www.ill.fr/dif/ccsl/html/ccsl/doc.html>
²⁴ J. P. C. Ruff *et al.* *Phys. Rev. Lett.* **99**, 237202 (2007).
²⁵ S.-W. Han, J. S. Gardner, C. H. Booth, *Phys. Rev. B* **69**, 024416 (2004).
²⁶ I. V. Aleksandrov *et al.* *Sov. Phys. JETP* **62**, 1287 (1985).
²⁷ A. Apetrei *et al.* *J. Phys. Cond. Mat.* **19**, 376208 (2007).